

Mapping Middle Triassic Doig Sandstone Reservoirs in Northeast British Columbia Using Seismic Attributes*

Satinder Chopra¹, Ritesh Kumar Sharma², and James Keay²

Search and Discovery Article #51080 (2015)

Posted April 6, 2015

*Adapted from extended abstract prepared in conjunction with an oral presentation given at the 2014 GeoConvention, Calgary, Alberta, Canada, May 12-16, 2014, GeoConvention/Datapages © 2015

¹Arcis Seismic Solutions, TGS, Calgary (schopra@arcis.com)

²Arcis Seismic Solutions, TGS, Calgary

Abstract

The Doig sandstone reservoirs have historically produced oil and gas in northeast British Columbia and northwest Alberta, Canada. These reservoirs occur in the study area as N-S trending linear sandstone geobodies 10-30 m in thickness at many places, and some tens of kilometers long. The challenge is the determination of the reservoir sands 20 m in thickness from seismic data that has an average bandwidth of 10-60 Hz. In the area under study, comprising the Fireweed, Buick Creek West, and the Stoddard areas in northeast British Columbia, the reactivation of the deeper fault structures also have some tectonic control on the Doig sandstones of interest. Therefore, the challenge is to identify not only the spatial variability of these Doig sands but also crosscutting faults and fractures.

We address these challenges by first enhancing the bandwidth of the available seismic data using spectral inversion to estimate thin bed reflectivity, followed by relative acoustic impedance and unconstrained waveform classification to map the reservoir heterogeneity. This is followed by generation of coherence and curvature attributes to detect minor faults and fractures.

Introduction

The Doig sandstone reservoirs in northeast British Columbia and northwest Alberta have historically produced oil and gas in these areas. The underlying Doig phosphate beds have more recently gained attention as producing wet gas reservoirs due to horizontal completion technology, along with the underlying Montney wet gas resource plays. The area under study comprises the Fireweed, Buick Creek West, and the Stoddard areas in northeast British Columbia. Sandstones in these areas were deposited by sea level fluctuations on a low-relief marine shelf, where little structural deformation would be expected. Subsequent reactivation of the deeper fault structures appears to have some tectonic control on the Doig sandstones.

In the area under study ([Figure 1](#)), Doig sandstones are expected as north-south trending linear sand geobodies 10-20 m thick (up to 30 m at some places), and some tens of kilometers long. The challenge is the determination of the reservoir sands 20 m in thickness from seismic data that has an average bandwidth of 10-60 Hz. This would help with the placement of the wells and hence the development of the area.

A workflow comprising first the enhancement of the bandwidth of the seismic data, followed by the generation of seismic attributes aimed at characterizing the variation in the quality of the sand reservoirs and the discontinuities in the zone of interest was developed to address the challenge at hand.

Geological Setting and Background

The Middle Triassic Doig Formation of Western Canada is seen to occur in north-western Alberta, north-eastern British Columbia and southern Yukon provinces of Canada and is composed of argillaceous siltstone and calcareous shale. It is unconformably overlain by the Halfway Formation ([Figure 1](#)) and itself overlays the Montney Formation. While the maximum thickness of the Doig Formation reaches over 180 m in the foothills of the Rocky Mountains, it thins out to the north and the east. Within the Doig Formation, thick sandstone bodies occur, and many of them are found to be economic hydrocarbon reservoirs; hence the attraction for their exploration and development. Examination of the available core from the Doig sandstone reservoirs suggests an association between sedimentary facies such as shoreface, offshore transition, and offshore/shelf. Phosphates and other accessory minerals in the Doig sandstone bodies can drive the gamma ray tool response and mask the sands, so correct identification of the bodies on logs requires multiple curves. The facies change quickly in both the vertical and the horizontal directions. Recognition of these facies changes and characterization of the Doig sandstones serves as a useful input for exploration and development purposes.

Seismic Data Interpretation

As the first step towards interpretation, the available log curves were correlated with the seismic data. The impedance logs as well as the synthetic seismograms were overlaid on the seismic data and were found to be matching reasonably well. One such correlation is shown in [Figure 2](#). The Doig sandstone exhibits higher impedance than the shale unit below it and so seen as a peak on the seismic response. However, as the thickness of the Doig sand varies, this peak may not be present everywhere.

The overlay of the impedance log curve on a segment of a section from the 3D seismic data volume is shown in Figure 3. The Doig sand is indicated on this display as the yellow horizon segments ([Figure 3b](#)). The green horizon above was used to generate the strat-slice for displaying the areal extent of the Doig sandstone and will be referred to later.

The bandwidth of the seismic data does not seem to be broad enough to accurately determine the areal extent and thickness of the Doig sands in the range of 10-20 m in the study area. For this reason, the bandwidth of the data was enhanced and the method of choice was the thin-bed reflectivity, described in the next section (Chopra et al., 2006; Puryear and Castagna, 2008). This led to improved definition of the depositional architecture of the sandstones and helped to quantify the local definition on them.

As some structural deformation in the form of folds, faults, and fractures are expected in the zone of interest, coherence and curvature attribute volumes were generated. Finally, seismic facies mapping provides a definition of lateral variation of the reservoir sands and throws light on the understanding of the different units. For achieving this objective, unconstrained waveform classification (Chopra, 2012) was run around the zone of interest. These are described in the next section.

Characteristics of Doig Sandstones

Frequency Enhancement of Seismic Data

As described by Puryear and Castagna (2008), spectral inversion utilizes spectral decomposition to unravel the complex interference patterns created by thin-bed reflectivity. This inversion process does not require stringent assumptions for its performance, such as any *a priori* or starting earth model, nor any reflectivity spectrum assumptions beyond that implied by the assumption that the earth model is blocky, nor horizon constraints. Neither is a well constraint mandatory, though having one well control point can be helpful for wavelet extraction. For data with high signal-to-noise ratio (SNR), thicknesses far below tuning can sometimes be resolved.

The output of the inversion process can be viewed as spectrally broadened seismic data, retrieved in the form of broadband reflectivity data that can be filtered back to any bandwidth that filter panel tests indicate adds useful information for interpretation purposes. [Figure 3](#) shows a comparison of a segment of a seismic section from the 3D seismic volume under study and its equivalent filtered reflectivity section. Keeping in mind the quality of the input seismic data, the filtered thin-bed reflectivity section looks much better in terms of the noise level as well as extra reflection detail. Based on our trial and error experimentation, the reflectivity was filtered back to 110 Hz at the high end, compared to 70 Hz which was the high end frequency of the input data. This enhanced data was utilized for generating the seismic attributes and carrying out the interpretation.

Seismic Attribute Generation: Impedance Attributes

Impedance profiles can be represented as either absolute impedances, which have magnitudes equivalent to the magnitudes of log data measured across targeted intervals, or as relative impedances, which have arbitrary amplitudes that show depth dependent variations equivalent to those exhibited by log data. We emphasize here the advantage of calculating relative impedances from thin-bed reflectivity data (Chopra et al, 2009). When interpreting relative impedance profiles, the top and bottom reflection boundaries of a unit are not correlated with well log curves. Instead, the thicknesses of relative impedance layers are correlated with log curve shapes. [Figure 4](#) shows a comparison of the acoustic impedance inversion run on the input data, the filtered thin-bed reflectivity data, as well as the relative acoustic impedance run on the thin-bed reflectivity data. Notice, the higher resolution of impedance variation in [Figure 4b](#) and more focused definition of impedance detail in [Figure 4c](#).

Seismic Attribute Generation: Discontinuity Attributes

Volumetric computation of coherence and curvature are useful seismic discontinuity attributes that come in handy during interpretation. By first estimating the volumetric reflector dip and azimuth that represent the best single dip for each sample in the volume, followed by computation of coherence or curvature from adjacent measures of dip and azimuth, a full 3D volume of coherence/curvature values is produced. Besides coherence, many curvature measures can be computed, but the most-positive and most-negative curvature measures are perhaps the most useful in that they tend to be most easily related to geologic structures. Besides stratigraphic features such as levees and bars, and diagenetic features such as karst collapse and hydrothermally-altered dolomites also appearing well-defined on curvature displays, volumetric curvature attributes are valuable in mapping subtle flexures and folds associated with fractures in deformed strata.

[Figure 5](#) shows a chair display with seismic as the vertical slice and a strat-slice from the coherence attribute. Notice the areal extent of the Doig sandstone is seen clearly on the coherence as indicated with the green arrows and is correlated well with the seismic signature on the vertical slice indicated with the yellow arrows. In [Figure 6](#) we show the overlay of the most-positive and most-negative curvature attributes, using transparency, on the acoustic impedance on enhanced frequency seismic data. Notice how the black curvature lineaments fit in nicely with the distribution of the acoustic impedance patterns.

Seismic Attribute Generation: Unconstrained Waveform Classification

The shape and character of the seismic waveform is often used to characterize reservoir quality. This is because the seismic waveform carries information about the phase, frequency, and amplitude, and any variation in these parameters is considered reflective of the lateral variations in lithology, porosity, and fluid content. If the shape and character of seismic waveforms in a given target zone can be studied using some pattern recognition type of a process, and then displayed in a map view, the display would indicate seismic facies variation at the target level.

One approach to pattern recognition is with the use of neural networks to compare seismic waveforms and group them into different classes. Under this approach two types of methods could be distinguished, namely *unsupervised* and *supervised* classifications. In the unsupervised method, apart from defining an analysis interval, no other *a priori* information is used for the classification of seismic traces into groups or classes. The supervised method uses the known information available at specific well locations for the classification process. In this article, we discuss the unsupervised approach, which has been described recently by Chopra (2012).

Once a seismic facies map is generated using unsupervised waveform classification, it is possible to apply the process again to individual classes. In that sense, the process is *hierarchical* and subdivides each class into smaller subsets. Iteratively applying it enhances the resolution of each class. We selected an interval of 78 ms about the Doig sandstone in a horizon-consistent way as seen in [Figure 7](#). We begin with 4 classes and the facies variation is shown in [Figure 7a](#). Realizing that the number of classes chosen may not have yielded an optimum facies variation, next we decided to adopt the hierarchical waveform classification. So, we sub-divided class 1 into classes 5 and 6 and class 2 into classes 7 and 8 and the results are shown in [Figure 7d](#). Notice, this display shows an even distribution to all the colors within the sand boundary, and so can be considered a reasonable facies variation.

The above workflow enabled us to determine the distribution of the Doig sandstone in the zone of interest and we were able to study its reservoir quality in terms of its facies distribution as well as the acoustic impedance variation. The fault and fracture distribution also fit in very nicely in the facies and acoustic impedance variation.

Conclusions

The challenge to identify not only the spatial variability of the Doig sandstone in the study area but the distribution of the crosscutting faults and fractures was addressed by following the workflow described above. Enhanced resolution of the seismic data by way of thin-bed reflectivity inversion helped with the detailed mapping of seismic facies and improved definition of the reservoir sands. Relative acoustic impedance inversion on thin-bed reflectivity as well as absolute model-based acoustic impedance inversion indicated variations in the quality of the Doig sandstones that matched other well control. This variation resembled the facies variation determined based on seismic waveform classification. Coherence and curvature attributes indicated the local structural deformation in terms of folds, small faults and fractures. Such a seismic attribute workflow has enabled accurate characterization of the Doig sandstones.

Acknowledgements

We wish to thank Arcis Seismic Solutions, TGS, for encouraging this work and for permission to present these results.

References Cited

- Chopra, S., J.P. Castagna, and O. Portniaguine, 2006, Seismic resolution and thin-bed reflectivity inversion: CSEG Recorder, v. 31/1, p. 19-25.
- Chopra, S., J.P. Castagna, and Y. Xu, 2009, Thin is in: Here's a Helpful Attribute, AAPG Explorer, v. 7, p. 24.
- Chopra, S., 2012, Waveform classification proves itself a valuable tool, AAPG Explorer, v. 11, p. 54-55.
- Puryear, C.I., and J.P. Castagna, 2008, Layer-thickness determination and stratigraphic interpretation using spectral inversion: theory and application: Geophysics, v. 73, p. R37-R48.

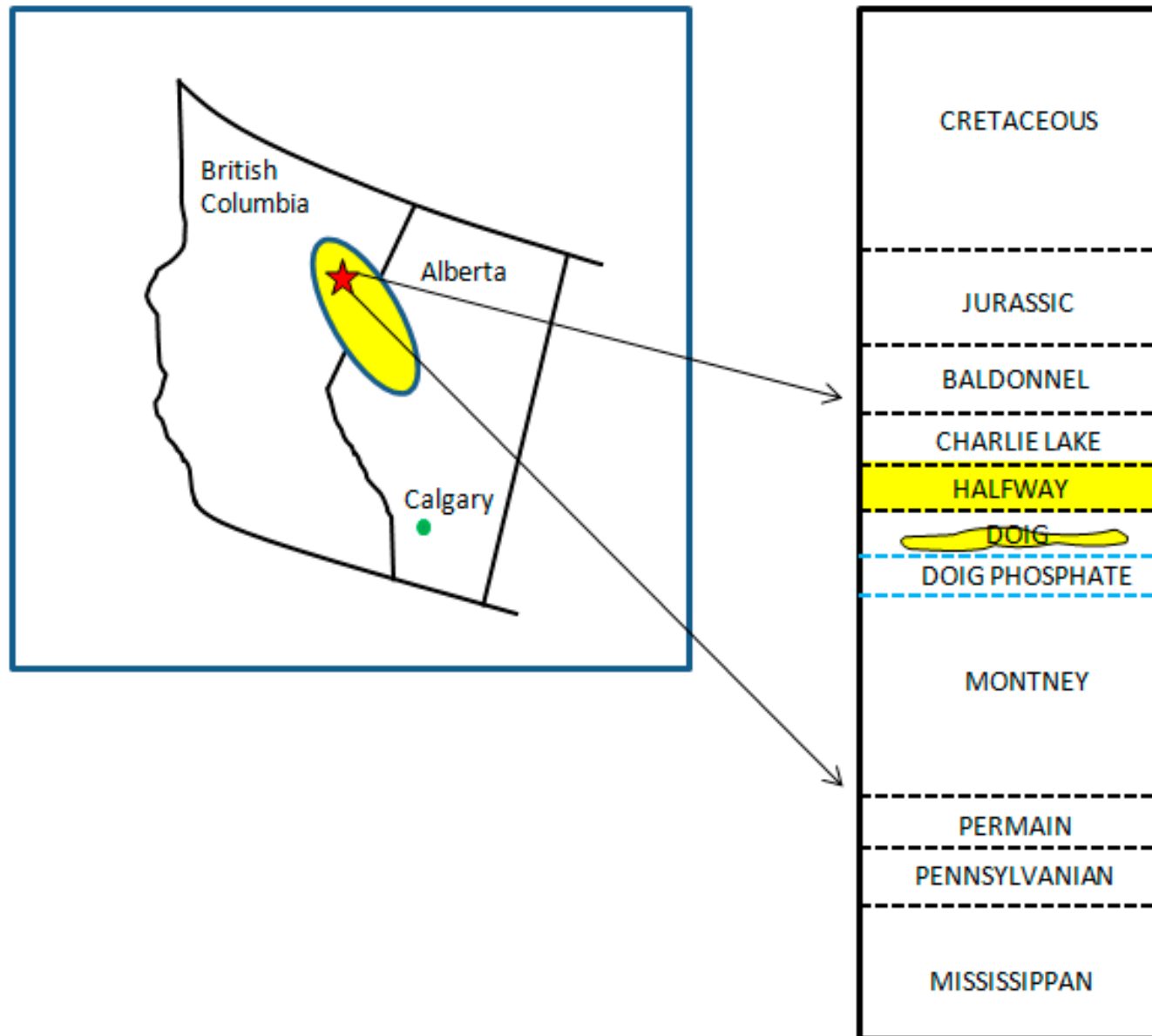


Figure 1. (a) Sketch map showing the Doig resource play (in yellow) in Western Canada spanning northeastern British Columbia and northwestern Alberta. The red star indicates the location of the study area. (b) The stratigraphic column for the zone of interest comprising the Halfway, Doig, Doig Phosphate, and the Montney.

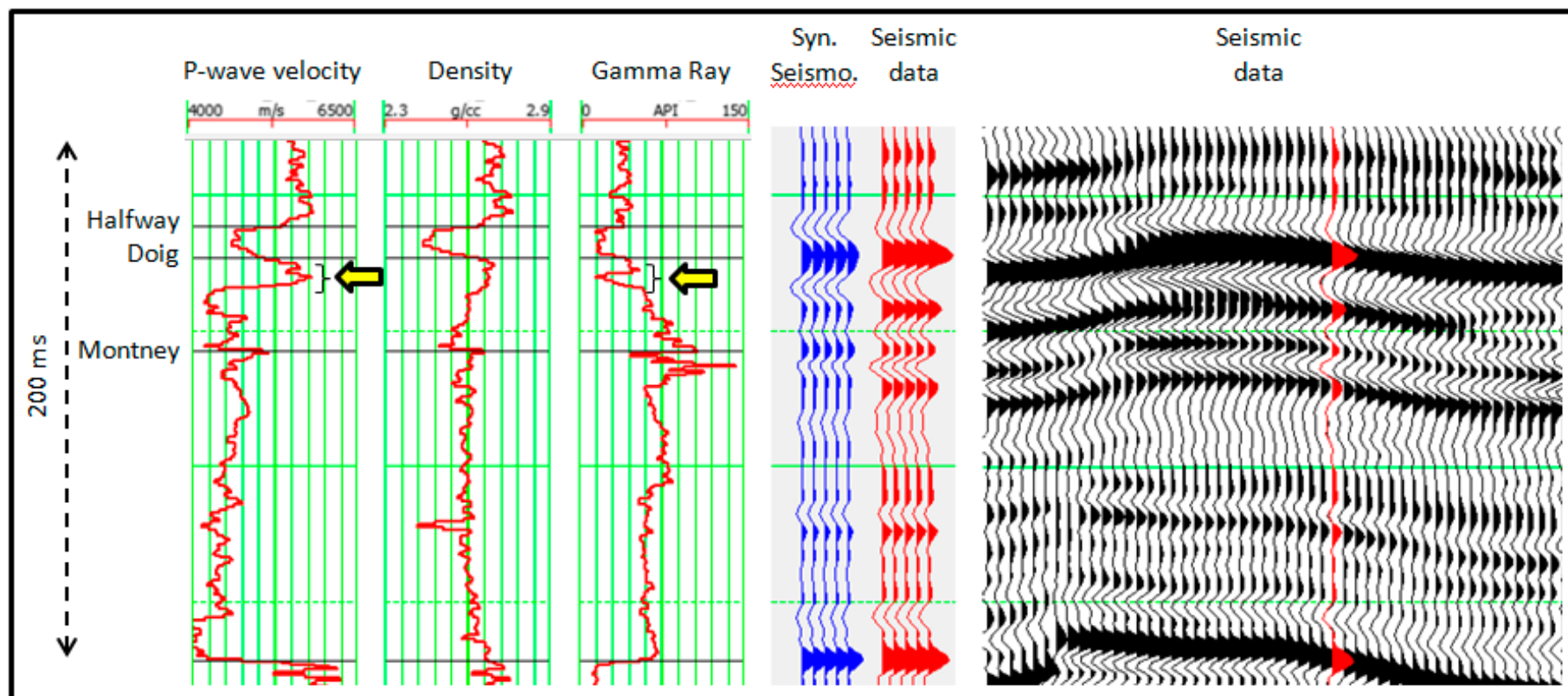


Figure 2. Correlation of well log curves with synthetic seismogram and seismic data. The Doig sand is indicated on the P-velocity curve with a yellow arrow.

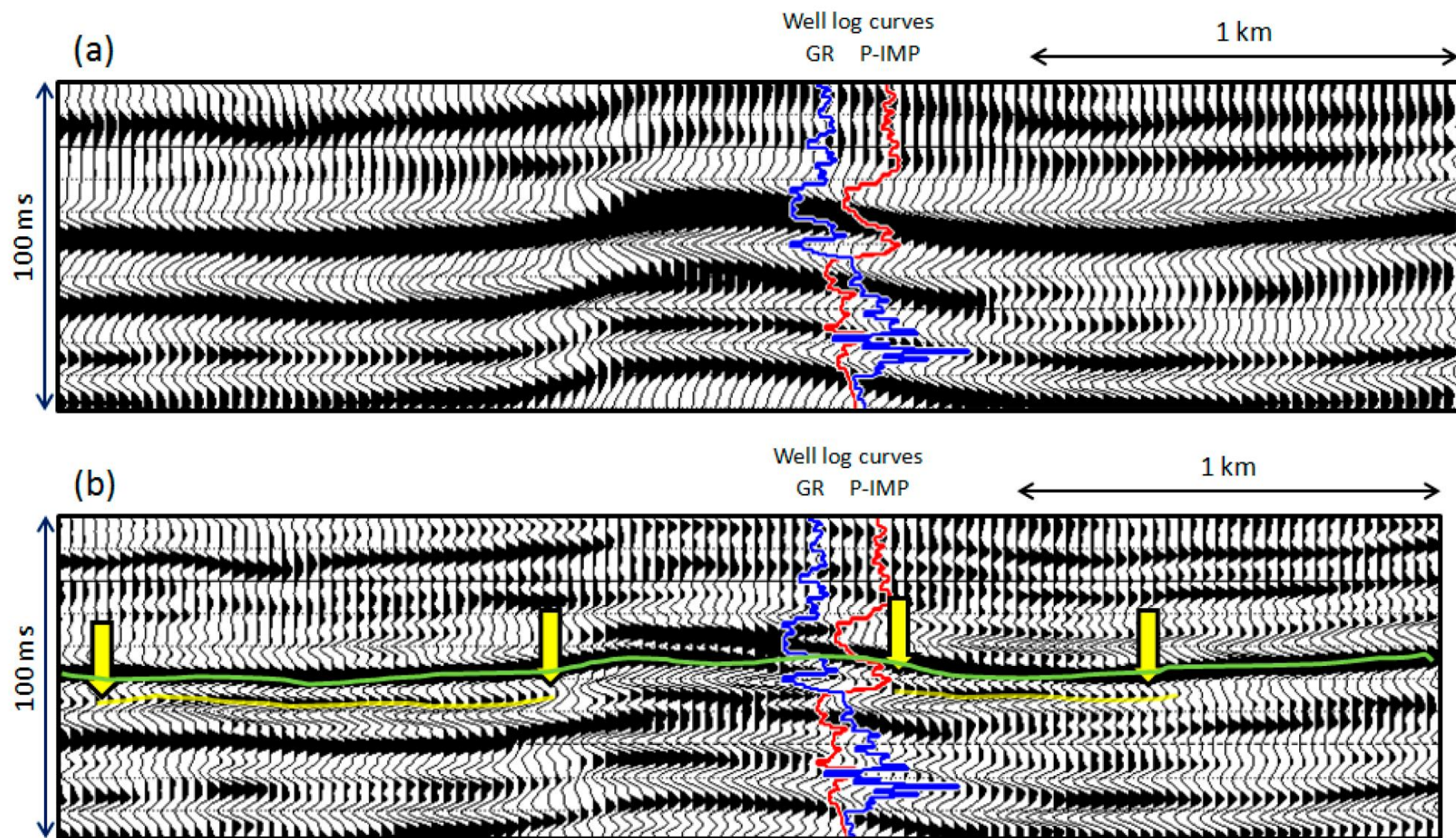


Figure 3. A segment of (a) the input seismic section, (b) the frequency enhanced seismic section (equivalent to the one shown in Figure 3a) passing through a well, with the GR and impedance logs overlaid on it. The signature of the Doig sand is marked with the yellow dashed horizon segment as well as the yellow arrows.

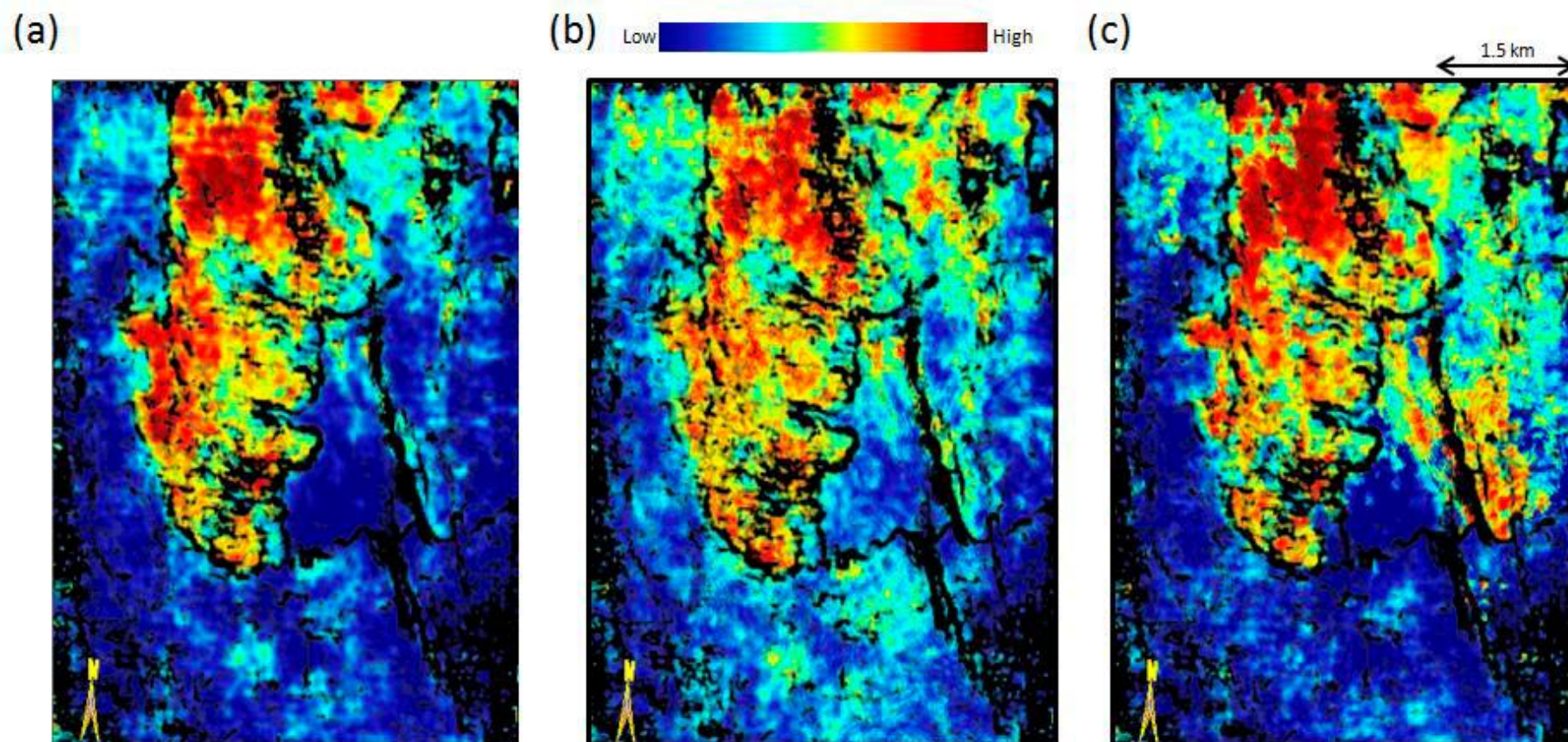


Figure 4. Strat-slices from the (a) absolute acoustic impedance volume run on the input seismic data, (b) absolute acoustic impedance volume run on the frequency enhanced seismic data by wave of thin-bed reflectivity inversion and filtering to a higher bandwidth than the input seismic data, and (c) relative acoustic impedance volume run on the thin-bed reflectivity, merged with the coherence attribute using transparency. The sandstone distribution is seen in terms of the high impedance pattern seen within the coherence. Notice the higher resolution in the sandstone distribution in (b) and more focused detail in (c).

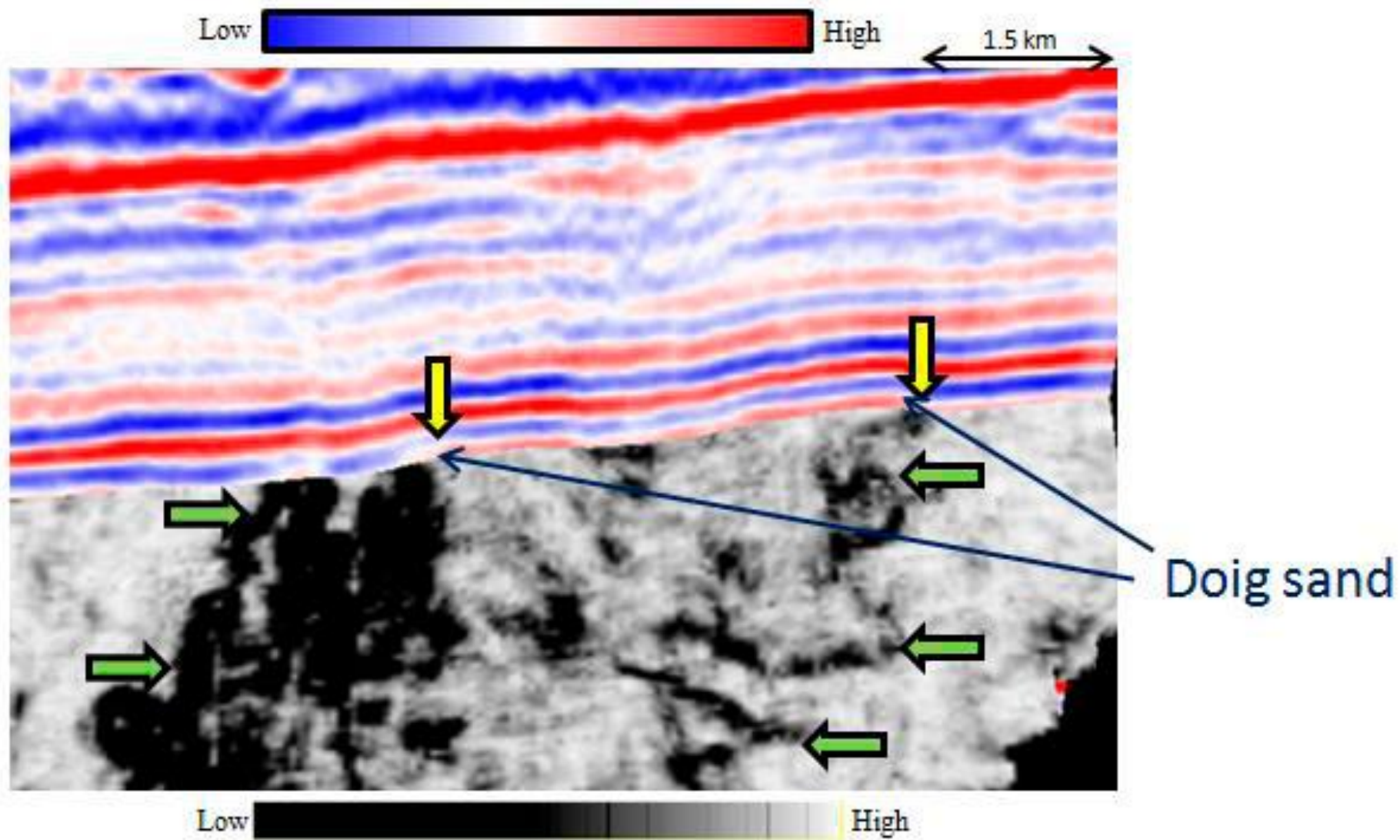


Figure 5. Chair display with the seismic as vertical and the coherence horizon slice indicating the extent of the Doig sand. The seismic signature of the Doig sand is seen clearly as indicated with the yellow arrows and its areal extent indicated with the green arrows.

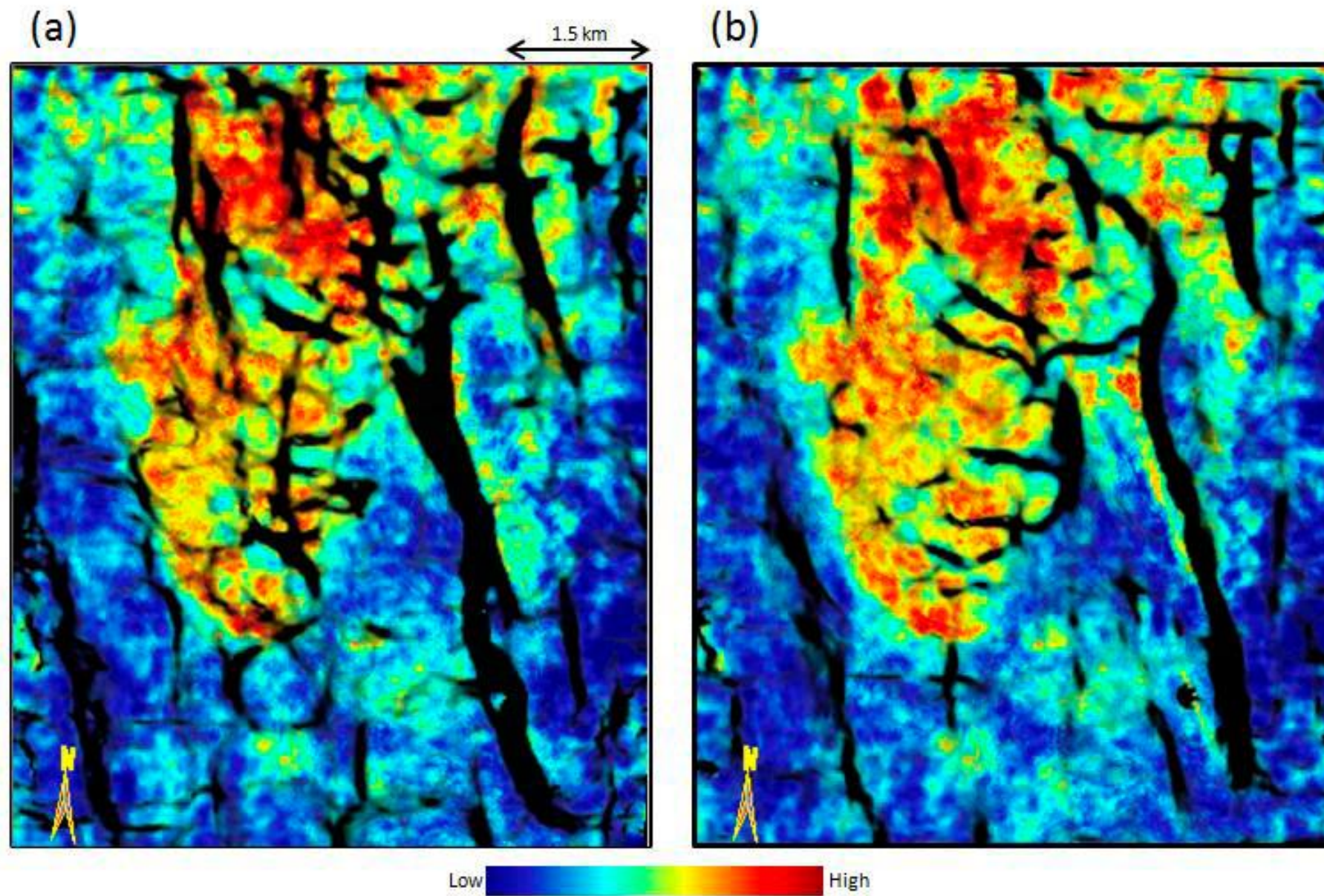


Figure 6. Strat-slice from the absolute acoustic impedance volume run on frequency enhanced seismic data with (a) most-positive curvature, and (b) most-negative curvature, overlaid using transparency.

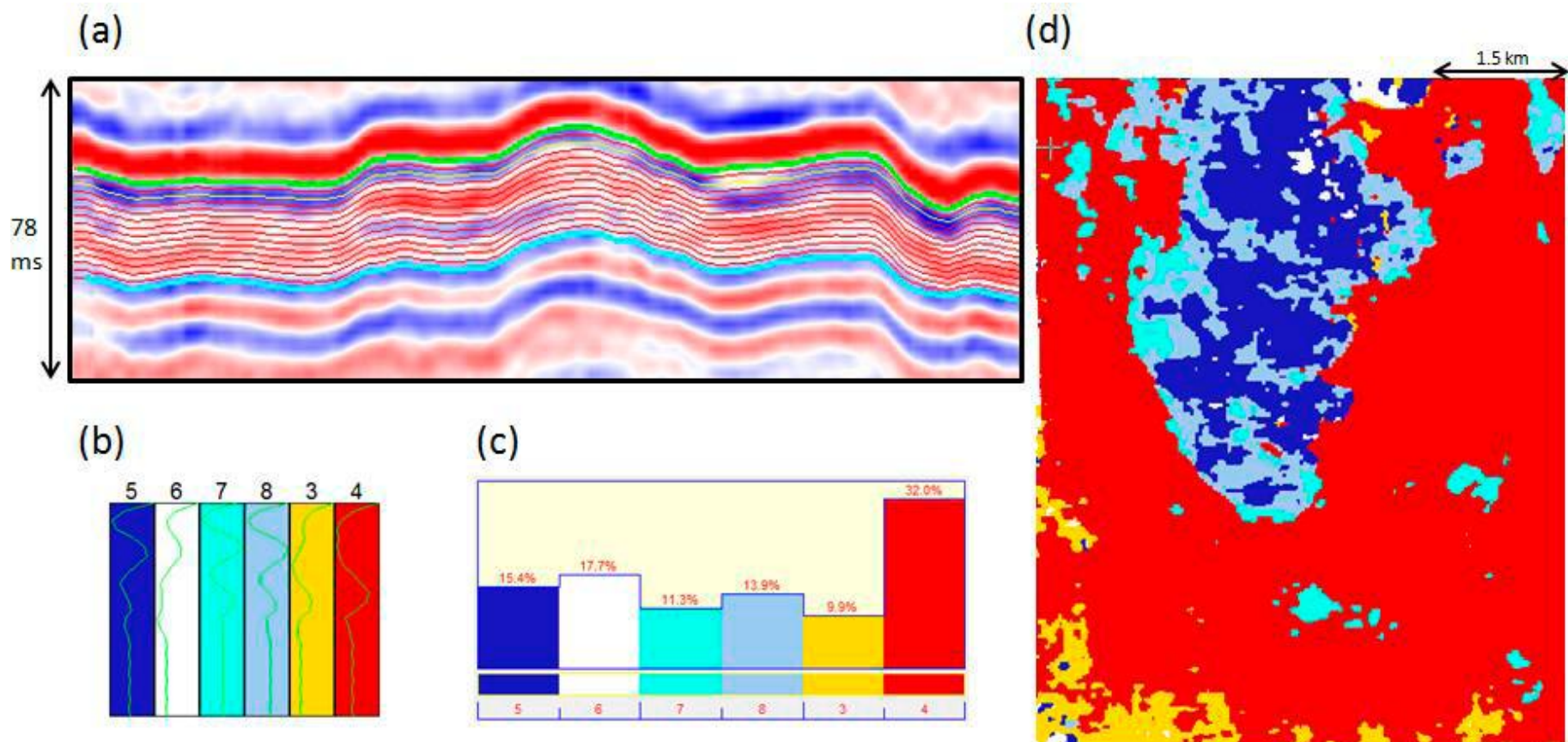


Figure 7. (a) A segment of the seismic section shows the interval (78 ms) that encloses the Doig sand and so is the zone of interval for waveform classification. (b) Hierarchical waveform classification is attempted using 4 classes wherein class 1 is subdivided into classes 5 and 6 and class 2 in turn subdivided into 7 and 8 as shown. Their individual contributions are shown as comparative percentages in (c). Notice the blue, cyan, and grey classes show the variation within the sand distribution as displayed in (d).